The structure of the liquid–vapor interface of a gallium–tin binary alloy

ARTICLE *in* THE JOURNAL OF CHEMICAL PHYSICS · JULY 1999

Impact Factor: 2.95 · DOI: 10.1063/1.479490

2 AUTHORS:

Meishan Zhao
University of Chicago
104 PUBLICATIONS **1,649** CITATIONS
SEE PROFILE

Stuart A. Rice
University of Chicago
712 PUBLICATIONS **22,026** CITATIONS
SEE PROFILE

The structure of the liquid-vapor interface of a gallium-tin binary alloy

Meishan Zhao and Stuart A. Rice

Citation: The Journal of Chemical Physics **111**, 2181 (1999); doi: 10.1063/1.479490
View online: http://dx.doi.org/10.1063/1.479490
View Table of Contents: http://scitation.aip.org/content/aip/journal/jcp/111/5?ver=pdfcov
Published by the AIP Publishing

The structure of the liquid-vapor interface of a gallium-tin binary alloy

Meishan Zhao and Stuart A. Rice
The James Franck Institute and Department of Chemistry, The University of Chicago, Chicago, Illinois 60637

(Received 15 January 1999; accepted 28 April 1999)

We report the results of self-consistent quantum Monte Carlo simulations of the structure of the liquid-vapor interface of the alloy $Sn_{0.09}Ga_{0.81}$. Our calculations are in very good agreement with the experimental results reported by Lei, Huang and Rice [J. Chem. Phys. **107**, 4051 (1997)]. In particular, our calculations confirm the experimentally inferred existence of a partial second layer of Sn below the complete outermost layer of Sn in the stratified liquid-vapor interface of this alloy. © *1999 American Institute of Physics.* [S0021-9606(99)70228-X]

I. INTRODUCTION

The major elements of our current theoretical understanding of the structure of the liquid-vapor interface of an alloy were first obtained from the results of calculations by Gryko and Rice,[1–3] and by Harris, Gryko and Rice.[4,5] They showed that in the liquid-vapor interface of a mixture of Cs and Na there are three important structural features. These are: (1) The distribution of the total ion density along the normal to the interface (the longitudinal density distribution) is stratified for 3–4 atomic diameters into the bulk liquid. (2) The segregation of Cs in the interface takes the form of a monolayer of pure Cs in the outermost layer of the liquid-vapor transition region. (3) There is a deficiency, relative to the bulk concentration, of Cs in the second layer of the stratified interface; the bulk concentration is reached in the fourth atomic layer.

The calculations reported by Harris, Gryko and Rice[4,5] are for the case that the alloy constituents have the same valence. Because electron density differences associated with ions of the same valence but different diameters are modest, the qualitative aspects of the structural features found in their calculations should be common to the class of homovalent alloys, irrespective of the valence. That this is so is verified by the results of grazing incidence x-ray diffraction and x-ray reflectivity studies of the liquid-vapor interface of a dilute alloy of Bi in Ga, reported by Rice and co-workers.[6,7] Their studies reveal that the excess Bi in the interface is concentrated in a monolayer that forms the outer layer of the interface. They also find that the Bi monolayer has the structure of a supercooled liquid, and that the stratification of the longitudinal density distribution of the underlying Ga host is sensibly the same as in pure Ga. Pershan and co-workers[8] have reported a similar set of studies of an alloy of In with Ga; they also conclude that the excess In concentration in the interface is concentrated in a monolayer that forms the outer layer of the interface. Calculations of the longitudinal density distributions in the BiGa and InGa alloy liquid-vapor interfaces, by Zhao, Chekmarev and Rice,[9,10] are in good agreement with the experimental data. The calculations of the structure of the liquid-vapor interface of InGa alloys[10] also reveal a deficiency of In atoms in the layer just below the outermost layer, just as predicted for CsNa alloys.[5]

The electron density differences associated with ions of different valences and different diameters are usually substantial, so we must expect some qualitative differences between the structures of the liquid-vapor interfaces of homovalent and heterovalent alloys. Indeed, the experimental studies of Lei, Huang and Rice[11] provide direct evidence that the atomic distribution in the liquid-vapor interface of a dilute SnGa alloy differs somewhat from the atomic distribution in the liquid-vapor interface of a dilute alloy of Bi in Ga. Specifically, unlike the atomic distribution in the liquid-vapor interface of the homovalent BiGa alloy, in the heterovalent SnGa alloy the excess Sn segregates into both the outermost and the second layers of the liquid-vapor interface; the outermost layer is pure two-dimensional liquid Sn, with an effective atomic diameter about 6% smaller than in bulk Sn at its (much higher) melting temperature, while the second layer has about 22% Sn, and there is not any detectable excess of Sn in any of the deeper layers. The source of the difference in the distributions of the surface active components in BiGa and SnGa alloys is attributed to the location of the outermost peak of the conduction electron density distribution between the first and the second ion layers in the liquid-vapor interface. Then, since the average conduction electron density of tetravalent liquid Sn is higher than that of trivalent liquid Ga, the top layer of the SnGa alloy liquid-vapor interface must have a larger electron density than that of pure Ga. Consequently, inclusion of some Sn atoms in the second atomic layer increases the conduction election density in that layer and thus reduces the overall electron density gradient in the interface, thereby decreasing the electron kinetic energy. In contrast, in the liquid-vapor interface of the BiGa alloy, the segregated Bi atoms form only one layer. Since the conduction electron density of trivalent liquid Bi is somewhat smaller than that of trivalent liquid Ga, adding Bi to the second layer of the liquid-vapor interface would decrease the conduction electron density in that layer and thereby increase the electron density gradient and the electron kinetic energy. This argument suggests that, in general, minimization of the conduction electron kinetic energy is an important factor in determining the distribution of excess concentration of a segregated component amongst the layers of the stratified liquid-vapor interface of an alloy.

This paper is concerned with the extension of self-

consistent quantum Monte Carlo simulations of the liquid alloy-vapor interface to the case of heterovalent alloys. The problem that must be addressed in making these calculations is the choice of reference background for the pseudopotential calculations. The valence difference between solute and host atoms in a dilute heterovalent alloy implies that the local charge density varies substantially as different ion core positions are sampled. It is not obvious, given the very strong dependence of the binding energy of an atom, and of the effective interaction between atoms, on the electron density, that the use of a homogeneous jellium reference distribution, such as employed in previously reported calculations, will adequately capture the interplay between the core potential and the electron density in an alloy with local variations in charge density.

The vehicle for our calculations is a study of the structure of the liquid-vapor interface of $Sn_{0.09}Ga_{0.81}$, since the structure of this interface has been reported.

II. BACKGROUND INFORMATION: EXPERIMENT

Lei, Huang and Rice[11] have studied the structure of the liquid-vapor interface of a $Sn_{0.09}Ga_{0.91}$ alloy by x-ray specular reflectivity and grazing incident x-ray diffraction. The results of these measurements were cited in the previous section. We now provide some previously unpublished details concerning the longitudinal density distributions of the Sn and Ga atoms in the liquid-vapor interface of the alloy.

The longitudinal electron density profile in the liquid-vapor interface, $n_e(z)$, averaged over a horizontal range that is the x-ray coherence length, is related to the specular x-ray reflectivity by

$$\frac{R(q_z)}{R_F(q_z)}=\left|\frac{1}{n_{e,\mathrm{bulk}}}\int_{-\infty}^{\infty}\frac{dn_e(z)}{dz}e^{iq_z z}dz\right|^2, \tag{1}$$

where $R_F(q_z)$ is the Fresnel reflectivity, and $n_{e,\mathrm{bulk}}$ is the average electron density in the bulk liquid. The longitudinal atomic density distributions of Sn and Ga, $\rho_{\mathrm{Sn}}(z)$ and $\rho_{\mathrm{Ga}}(z)$, are extracted from the electron density distribution by fitting to the convolution relation

$$n_e(z)=\int\{\rho_{\mathrm{Sn}}(z')f_{\mathrm{Sn}}(z-z')+\rho_{\mathrm{Ga}}(z')f_{\mathrm{Ga}}(z-z')\}dz', \tag{2}$$

where $f_{\mathrm{Sn}}(z)$ and $f_{\mathrm{Ga}}(z)$ are, respectively, the Fourier transforms of the atomic structure factors $f_{\mathrm{Sn}}(q_z)$ and $f_{\mathrm{Ga}}(q_z)$ for Sn and Ga. For the purpose of fitting the data, Lei, Huang and Rice represented the normalized longitudinal atomic densities of Sn and Ga by the functions

$$\frac{\rho_{\mathrm{Sn}}(z)}{\rho_{\mathrm{bulk}}}=\frac{\alpha}{\sigma_{\mathrm{Sn}}}e^{-(z+d_{\mathrm{Sn}})^2/2\sigma_{\mathrm{Sn}}^2}+\frac{\beta\beta'}{\sigma_0}e^{-z^2/2\sigma_0^2}+\sum_{j=1}^{\infty}\frac{0.09}{\sigma_j}e^{-(z-jd_{\mathrm{Ga}})^2/2\sigma_j^2}, \tag{3}$$

and

$$\frac{\rho_{\mathrm{Ga}}(z)}{\rho_{\mathrm{bulk}}}=\frac{\beta(1-\beta')}{\sigma_0}e^{-z^2/2\sigma_0^2}+\sum_{j=1}^{\infty}\frac{0.91}{\sigma_j}e^{-(z-jd_{\mathrm{Ga}})^2/2\sigma_j^2}, \tag{4}$$

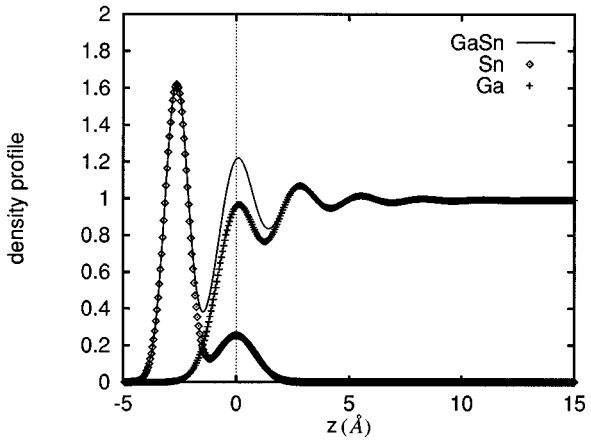

FIG. 1. The normalized experimental longitudinal atomic density profile of the liquid-vapor interface of $Sn_{0.09}Ga_{0.91}$ at $T=57\,^{\circ}\mathrm{C}$ and bulk density 0.0495 at./ $Å^3$.

subject to the constraint

$$\rho(z)=\rho_{\mathrm{Sn}}(z)+\rho_{\mathrm{Ga}}(z)=\frac{\alpha}{\sigma_{\mathrm{Sn}}}e^{-(z+d_{\mathrm{Sn}})^2/2\sigma_{\mathrm{Sn}}^2}+\frac{\beta}{\sigma_0}e^{-z^2/2\sigma_0^2}+\sum_{j=1}^{\infty}\frac{1}{\sigma_j}e^{-(z-jd_{\mathrm{Ga}})^2/2\sigma_j^2}. \tag{5}$$

In Eqs. (3) and (5), $\alpha=\rho_{\mathrm{outermost}}/\rho_{\mathrm{bulk}}$ is the ratio of the atomic density in the outermost layer of the stratified liquid-vapor interface to the density of the bulk liquid, $\beta=\rho_{\text{2nd-layer}}/\rho_{\mathrm{bulk}}$ is the ratio of the atomic density in the second outermost layer of the interface to the density of the bulk liquid, and $\beta'=0.22$ is the fractional concentration of Sn in the second layer of the interface. At $T=57\,^{\circ}\mathrm{C}$, the fitting parameters in Eqs. (3)–(5) are $d_{\mathrm{Sn}}=2.63$ Å , $d_{\mathrm{Ga}}=2.53$ Å , $\sigma_{\mathrm{Sn}}^2=0.367$ $Å^2$, $\sigma_{\mathrm{Ga}}^2=0.42$ $Å^2$, and

$$\sigma_j^2=\sigma_{\mathrm{Sn}}^2+(j+1)\sigma_{\mathrm{Ga}}^2,\quad j=0,1,\ldots\infty. \tag{6}$$

Then

$$\alpha=\frac{\rho_{(100\%\mathrm{Sn})}}{\rho_{(9\%\mathrm{Sn};\ 91\%\mathrm{Ga})}}=\frac{0.09r_{\mathrm{Sn}}^3+0.91r_{\mathrm{Ga}}^3}{r_{\mathrm{Sn}}^3}=0.8363, \tag{7}$$

$$\beta=\frac{\rho_{(22\%\mathrm{Sn};\ 78\%\mathrm{Ga})}}{\rho_{(9\%\mathrm{Sn};\ 91\%\mathrm{Ga})}}=\frac{0.09r_{\mathrm{Sn}}^3+0.91r_{\mathrm{Ga}}^3}{0.22r_{\mathrm{Sn}}^3+0.78r_{\mathrm{Ga}}^3}=0.9728, \tag{8}$$

where r_{Sn} and r_{Ga} are, respectively, the atomic radii of Sn and Ga. Lei, Huang and Rice also reported measurements of the structures and related properties of the same $Sn_{0.09}Ga_{0.91}$alloy at $T=12$, 26 and 47 °C. Figure 1 shows the experimental longitudinal atomic density profile in the liquid-vapor interface of $Sn_{0.09}Ga_{0.91}$at $T=57\,^{\circ}\mathrm{C}$.

III. BACKGROUND INFORMATION: THEORY

A. System Hamiltonian of liquid binary alloys

We have carried out our analysis of the structure of liquid and liquid-vapor interface using the pseudopotential rep-

resentation developed by Rice *et al.*[1–5,9,10,12–18] The details of the formal theory can be found elsewhere.[9] In this paper we sketch only those aspects of the theory required for the reader to understand the calculations reported.

The pseudopotential Hamiltonian has the form

$$\mathbf{H}=\sum_{i=1}^{N}\frac{\mathbf{p}_i^2}{2m}+\sum_{i=1}^{N}\sum_{j<i}\phi_{\mathrm{eff}}(|\mathbf{R}_i-\mathbf{R}_j|;n_e(\mathbf{r}))+U_0[\rho_0(\mathbf{r}),n_e(\mathbf{r})], \tag{9}$$

where $\mathbf{p}_i$ is the momentum of the ith atom with mass m, $\phi_{\mathrm{eff}}(|\mathbf{R}_i-\mathbf{R}_j|;n_e(\mathbf{r}))$ is the effective pair potential between ions i and j,

$$R=|\mathbf{R}_i-\mathbf{R}_j| \tag{10}$$

is the distance between atom i and atom j, and $\rho_0(\mathbf{r})$ and $n_e(\mathbf{r})$ are reference jellium and electron densities. The functional $U_0[\rho_0(\mathbf{r}),n_e(\mathbf{r})]$ is a structure independent contribution to the energy which is, however, dependent on the electron and jellium densities. We use atomic units for all physical quantities in the following discussion, unless specified otherwise.

The ion-ion pair potential in the inhomogeneous liquid metal is calculated using a local density approximation and the ion-ion pair potential of the homogeneous liquid metal,

$$\phi_{\mathrm{eff}}=\phi_H(R;\tfrac{1}{2}[n_e(\mathbf{R}_i)+n_e(\mathbf{R}_j)]). \tag{11}$$

In a homogeneous liquid metal with electronic density $n_e(\mathbf{r})$ the pair interaction is

$$\phi_H(R)=\frac{z_i^*z_j^*}{R}\left\{1-\frac{1}{\pi}\int_0^\infty[F_{ij}(q)+F_{ji}(q)]\frac{\sin(qR)}{q}dq\right\}+\phi_{\mathrm{BM}}(R)+\phi_{vw}(R). \tag{12}$$

The first term in Eq. (12) is due to the direct Coulomb repulsion between ions with effective valence charges z_i^* and z_j^*. The second term is an indirect interaction mediated by the conduction electrons, the so-called band structure energy. This potential term tends to offset the effect of the strong Coulomb repulsion and thus lowers the energy of the system. $\phi_{\mathrm{BM}}(R)$ is the Born-Mayer core-core repulsion interaction,[19]

$$\phi_{\mathrm{BM}}(R)=A_{\mathrm{BM}}e^{-B_{\mathrm{BM}}R}, \tag{13}$$

where A_{BM} and B_{BM} are the Born-Mayer potential parameters, and $\phi_{\mathrm{vw}}(R)$ is the van der Waals polarization interaction between the ion cores.[2] In general, both $\phi_{\mathrm{BM}}(R)$ and $\phi_{vw}(R)$ are much smaller than the other terms contributing to the energy of the liquid metal.

The effective valence charges z_i^* and z_j^* are defined by

$$z_i^*z_j^*=Z_iZ_j-\overline{Z}_i\overline{Z}_j, \tag{14}$$

where Z is the true valence charge and $\overline{Z}$ is the depletion hole charge that originates from the orthogonality condition between the valence and core electron wave functions.

The normalized energy wave-number characteristic function $F_N(q)$, as derived by Shaw,[20] is

$$F_{ij}(q)=\frac{\Omega^2q^4}{16\pi^2z_i^*z_j^*}\left\{\frac{[1-\epsilon(q)](v_1+v_2)^2}{\epsilon(q)}+2g(q)(v_1+v_2)+\epsilon(q)g(q)^2+h(q)\right\}, \tag{15}$$

where $\Omega=(\rho_{\mathrm{bulk}})^{-1}$ is the volume per atom, ρ_{bulk} is the bulk liquid density, $\epsilon(q)$ is the wave-number dependent Hartree dielectric function, $g(q)$ is a nonlocal screening function, and $h(q)$ is a nonlocal bare pseudopotential contribution to the second order approximation. The local potential contributions v_1 and v_2, arising from the valence charge Z and the depletion hole charge $\overline{Z}$, are given by

$$v_1=-\frac{2\pi}{\Omega q^2}(Z_i+Z_j), \tag{16}$$

$$v_2=-\frac{2\pi}{\Omega q^2}(\overline{Z}_i+\overline{Z}_j). \tag{17}$$

The structure-independent energy $U_0[\rho_0(\mathbf{r}),n_e(\mathbf{r})]$ is a functional of both the reference jellium density and the electronic density; it has the form

$$U_0[\rho_0(\mathbf{r}),n_e(\mathbf{r})]=\frac{3(3\pi^2)^{2/3}\sigma}{10}\int_0^\infty[n_e(\mathbf{r})]^{5/3}dz+\frac{\sigma}{72}\int_0^\infty\frac{|\nabla^2n_e(\mathbf{r})|}{n_e(\mathbf{r})}dz$$
$$+\frac{\sigma}{540(3\pi^2)^{2/3}}\int_0^\infty dz[n_e(\mathbf{r})]^{2/3}\left[\left(\frac{\nabla^2n_e(\mathbf{r})}{n_e(\mathbf{r})}\right)^2-\frac{9}{8}\left(\frac{\nabla^2n_e(\mathbf{r})}{n_e(\mathbf{r})}\right)\left(\frac{\nabla n_e(\mathbf{r})}{n_e(\mathbf{r})}\right)^2+\frac{1}{3}\left(\frac{\nabla n_e(\mathbf{r})}{n_e(\mathbf{r})}\right)^4\right]^2$$
$$-2\pi\sigma\int_0^\infty dz\int_0^\infty dz'[\rho_0(z)\rho_0(z')-n_e(z)n_e(z')]|z-z'|$$
$$+2\sigma\int_0^\infty n_e(z)\varepsilon_{xc}[n_e(z)]dz+2\sigma\int_0^\infty\rho_0(z)\varepsilon_{ps}[n_e(z)]dz. \tag{18}$$

The first three terms of this equation are, respectively, the Fermi-Thomas uniform density contribution to the kinetic energy of a liquid metal with surface area σ, the von Weisacker first density correction to the kinetic energy of the inhomogeneous electron gas,[21] and the Kirzhnits second order gradient correction to the kinetic energy of the inhomogeneous electron gas.[22] The fourth term is the electrostatic energy of the system that arises from the difference between the electron and ion density distributions in the liquid-vapor transition zone, and the fifth term is the exchange-correlation contribution to the energy in the representation proposed by Vosko[23] with inclusion of the density gradient correction proposed by Langreth.[24] The last term is the electron-ion pseudopotential contribution to the electronic energy, with $\varepsilon_{ps}[n_e(z)]$ the ionic pseudopotential (which is a function of the electron density distribution).

The major difference in the pseudopotential representations of a pure metal and a binary alloy is found to be in the structure-independent energy $\varepsilon_{ps}[n_e(z)]$. For a binary alloy we have[2,10]

$$\varepsilon_{ps}=\frac{3}{k_F^3}\int_0^{k_F} f(q,q)q^2dq - \frac{1}{\pi}\sum_{i=1}^{2} X_i\int_0^{\infty} dq\{\overline{Z_i^2}|M_i(q)|^2-(z_i^*)^2F_{ii}(q)\} - \frac{2\pi}{\Omega}\sum_{i=1}^{2}\sum_{j=1}^{2} z_i^*z_j^*X_iX_j\lim_{q\to 0}\frac{1-F_{ij}(q)}{q^2} + \left(\frac{\alpha}{r_s}+\frac{\beta}{r_s}\right), \tag{19}$$

where k_F is the Fermi wave number, $f(q,q)$ is the diagonal matrix element of the Fourier transform of the nonlocal bare electron-ion pseudopotential $V_{ps}^{\text{ion}}(r)$, $M_i(q)$ is the Fourier transform of the depletion hole distribution, X_i is the mole fraction of the ith component and r_s is the radius of a sphere per unit electron that is determined from

$$\frac{1}{n_{e,\text{bulk}}}=\frac{4\pi}{3}r_s^3, \tag{20}$$

where $n_{e,\text{bulk}}$ is the bulk electron density of the liquid. The parameters α and β in Eq. (19) were determined by imposing the requirement that the calculated and observed pressure and heat of vaporization agree with experimental values at the liquid density.

B. Electron-ion pseudopotential

There are many different electron-ion pseudopotentials reported in the literature. We employed the nonlocal energy independent model pseudopotential proposed by Woo, Wang and Matsuura.[25] This potential has been previously used by Rice *et al.*[9,10,12–18] in studies of the structures of various pure liquid metals and binary alloys. It has the form

$$V_{ps}^{\text{ion}}(r)=\sum_l \{\overline{V}_l(r)+[V_{1l}(r)-\overline{V}_l(r)]|R_{1l}\rangle\langle R_{1l}|\}|l\rangle\langle l|, \tag{21}$$

TABLE I. Ionic pseudopotential parameters (in atomic units a.u.) $r_{\max}$ is the maximum value of r in the radial wave function.

	l	E_{1l}	R_l	B_{1l}	$r_{\max}$
Ga	0	1.128 60	1.941 04	1.546 51	35.0
	1	1.105 06	0.534 97	4.344 04	45.0
	2	0.472 14	2.023 58	0.335 13	55.0
Sn	0	1.120 927	0.911 00	4.430 40	35.0
	1	0.526 250	1.474 50	2.712 00	45.0
	2	0.269 887	5.332 00	4.819 60	55.0

where $\overline{V}_l(r)$ is a pseudopotential average over all states other than the first valence state for a given angular momentum l [$\overline{V}_l(r)$ is calculated in the same fashion as is $V_{1l}(r)$ except for replacing the parameter B_{1l} with $\overline{B}_{1l}$]. In (21), $|R_{1l}\rangle$ is the radial part of the wave function for the state $|1l\rangle$, and $|l\rangle$ is a simple projection onto the state with angular momentum l. With these definitions the model pesudopotential takes the form

$$V_{1l}(r)=\begin{cases} -B_{1l}+Z_l/r, & r\leqslant R_l; \\ Z_l/r, & r>R_l, \end{cases} \tag{22}$$

where B_{1l}, Z_l, R_l are parameters; they are usually determined by a pseudo-eigenfunction expansion and perturbation theory. Z is the valence of the ion. The state $|1l\rangle$ is separated into radial and angular parts, such that

$$\langle \mathbf{x}|1l\rangle=N\frac{1}{r}y_{1l}(r)Y_{lm}(\theta,\phi), \tag{23}$$

where N is a normalization constant, $Y_{lm}(\theta,\phi)$ is a spherical harmonic function, and $y_{1l}(r)$ is the radial wave function given by

$$y_{1l}(r)=\begin{cases} M_{\nu,l+1/2}(2\lambda r), & r\leqslant R_l; \\ W_{\nu_0,l+1/2}(2\lambda_0 r), & r>R_l, \end{cases} \tag{24}$$

where $M_{\nu,l+1/2}(2\lambda r)$ and $W_{\nu_0,l+1/2}(2\lambda_0 r)$ are, respectively, the regular and irregular Whittacker functions. The parameters of the Whittacker functions are

$$\lambda_0=\sqrt{-2E_{1l}}, \tag{25}$$

$$\lambda=\sqrt{-2(E_{1l}+B_{1l})}, \tag{26}$$

$$\nu_0=\frac{Z_l}{\sqrt{-2E_{1l}}}, \tag{27}$$

$$\nu=-\frac{Z_l}{\sqrt{-2(E_{1l}+B_{1l})}}, \tag{28}$$

with E_{1l} the spectroscopic term energy of the state $|1l\rangle$. The potential parameters we have used for our study of the structure of the liquid-vapor interface of the SnGa alloy are displayed in Table I. We show, in Fig. 2, the effective ion-ion pair interaction potentials.

C. Character of the jellium background

A key issue that must be addressed in the pseudopotential theory of heterovalent alloys is finding an appropriate

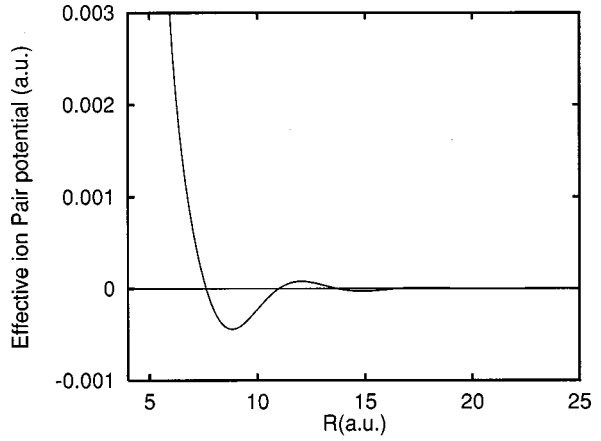

FIG. 2. The effective ion-ion pair interaction potential in liquid $Sn_{0.09}Ga_{0.91}$ at a density of 0.0495 at./Å^3.

representation of the jellium background. The choice of representation is important because the jellium background defines the reference atomic density profile in the pseudoatom Hamiltonian.

When the alloy is homovalent, it is appropriate to use the simplest uniform continuum representation of the charge density since there are only small differences between the local charge densities in the immediate neighborhoods of different ion cores of the same valence. Then the jellium distribution in the liquid-vapor interface can be represented by a simple functional form with parameters that are varied in the course of the calculation to achieve self-consistency between the electron and ion core distributions. In our previous work we used the functional form[4,5,9,10]

$$\rho(z,z_0,\beta)=\rho_{\text{bulk}}\left[1+\exp\left(\frac{|z|-z_0}{\beta}\right)\right]^{-1}. \tag{29}$$

Equation (29) represents the charge distribution of a slab of ions with two surfaces perpendicular to the z axis, where z_0 is the position of the Gibbs dividing surface and β measures the width of the inhomogeneous region of the profile. This distribution is normalized by setting $\rho_{\text{bulk}}=N/2\sigma z_0$, where N is the total number of atoms in the slab and σ is the area of the slab. The parameters z_0 and β are varied to obtain the best fit to the instantaneous ionic configuration.

When the alloy is heterovalent there can be large differences between the local charge densities in the immediate neighborhoods of different ion cores with different valence. In this case it is not immediately obvious that the use of the simplest uniform continuum representation of the charge density will provide an adequate basis for calculation of the interactions and the self-consistent electron and ion core density profiles in the liquid-vapor interface of the alloy. Nevertheless, we have used the effective valence approximation in the representation of the jellium distribution as a first approximation. The electron density obtained by using the effective valence representation will deviate to some extent from the true electron density. The needed correction to the electron density can be obtained self-consistently by iteratively re-solving the Kohn-Sham equation[26,27] (see below) using the simulated atomic density as the input. We expect that this approximation will be useful in the description of alloys which do not exhibit complex (A_nB_m) compound formation. The effective valence approximation should be accurate when the alloy exhibits 1:1 compound formation since then the compound-forming liquid has, effectively, the mean valence of the bulk liquid.

We define the effective valence in the binary alloy to be[28]

$$\overline{Z}=c_1Z_1+c_2Z_2, \tag{30}$$

where c_1 and c_2 are the atomic fractions of the two components. The bulk liquid mean electron number density is then

$$n_{e,\text{bulk}}=(c_1Z_1+c_2Z_2)\rho_b=\overline{Z}\rho_b, \tag{31}$$

where ρ_b is the bulk liquid atomic number density. In the case discussed in this paper, $c_1=0.91$ for Ga, and $c_2=0.09$ for Sn.

Our analysis of the heterovalent alloy liquid-vapor interface starts with the effective valence jellium and the reference profile displayed in Eq. (29), then calculates the electron density distribution from self-consistent solutions to the Kohn-Sham equation proposed by Eguiluz *et al.*,[29,30]

$$\left[-\frac{\hbar}{2m}\nabla^2+V_{\text{eff}}(\mathbf{r})\right]\psi_n(z)=E_n\psi_n(\mathbf{r}), \tag{32}$$

where $V_{\text{eff}}(\mathbf{r})$ is an effective potential that includes the electron-jellium background pseudopotential interaction $V_{ps}(\mathbf{r})$, the exchange-correlation potential $V_{xc}(\mathbf{r})$, and the electrostatic potential,

$$V_{\text{eff}}(\mathbf{r})=V_{ps}(\mathbf{r})+V_{xc}(\mathbf{r})+\int d\mathbf{r}\frac{n_e(\mathbf{r})}{|\mathbf{r}-\mathbf{r}'|}. \tag{33}$$

The exchange-correlation potential $V_{xc}(\mathbf{r})$ is defined as the derivative

$$V_{xc}(\mathbf{r})=\frac{\delta E_{xc}[n_e(\mathbf{r})]}{\delta n_e}, \tag{34}$$

where $E_{xc}[n_e(\mathbf{r})]$ is the exchange and correlation energy functional, and the electron number density is calculated from

$$n_e(\mathbf{r})=\sum_{n=1}^{\infty} f_n|\psi_n(\mathbf{r})|^2, \tag{35}$$

with f_n the electron occupation number in state $|\psi_n(\mathbf{r})\rangle$.

In our slab geometry the ion density distributions in the x and y directions are uniform, hence the electronic wave function $\psi_n(\mathbf{r})$ takes the form

$$\psi_n(\mathbf{r})=e^{i(k_xx+k_yy)}\phi_n(z), \tag{36}$$

where k_x and k_y are the wave numbers in the x and y directions, respectively. The electron density is then a function only of position along the normal to the interface, $n_e(\mathbf{r})\equiv n_e(z)$, and is obtained by solving the one-dimensional Kohn-Sham equation

$$\left[-\frac{\hbar}{2m}\frac{d^2}{dz^2}+V_{\text{eff}}(z;n_e(z))\right]\phi_n(z)=\epsilon_n\phi_v(z), \tag{37}$$

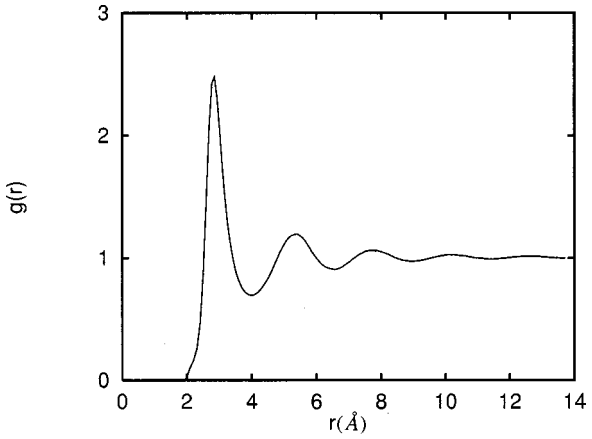

FIG. 3. A typical mean valence electron density profile in liquid $Sn_{0.09}Ga_{0.91}$ superposed on the jellium reference density at 0.0495 at./Å^3.

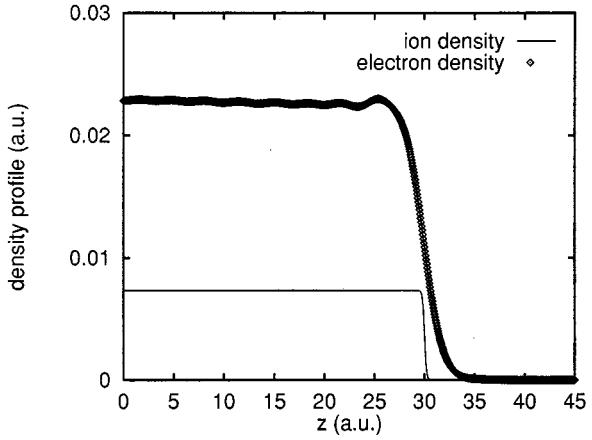

FIG. 4. Transverse pair correlation function of bulk liquid $Sn_{0.09}Ga_{0.91}$ at a density of 0.0495 at./Å^3 and $T=57$ °C.

$$E_n=\frac{\hbar^2}{2m_e}(k_x^2+k_y^2)+\epsilon_n, \quad n=1,2,\ldots \quad . \tag{38}$$

The result is

$$n_e(z)=\sum_{v=1}^{\infty} f_v|\phi_v(z)|^2, \tag{39}$$

with which we construct the electron density dependent potential $V_{\text{eff}}(z;n_e(z))$, and iterate the procedure until a self-consistent solution is obtained.

Figure 3 shows a typical mean valence electron density imposed on the jellium reference density.

D. Self-consistent quantum Monte Carlo simulations

All of the preceding refers to the calculation of the electronic energy and the effective ion-ion interaction associated with a particular ionic configuration in the inhomogeneous liquid metal. Of course, in the system of interest to us the ions are mobile, and a suitable average over all allowed ionic configurations must be calculated in order to determine the longitudinal and transverse density distributions in the liquid-vapor interface. As described above, an assumed initial jellium distribution is used to generate an electronic density distribution from which the ion-electron pseudopotential and effective ion-ion interaction potentials are calculated. The initial jellium distribution is then used in a Monte Carlo simulation of the inhomogeneous liquid-vapor system. Since each Monte Carlo step changes the ion distribution, it also changes the electronic density distribution, hence the ion-electron pseudopotential and the effective ion-ion interaction; this effect is particularly important in the inhomonegenous liquid-vapor transition zone. Accordingly, when the ion distribution is changed, the electron distribution is recalculated, to be consistent with the new ion distribution; this procedure is continued until the Monte Carlo simulation converges.

The most primitive way of carrying out the program is to repeat the calculations of the effective ion-ion interaction for every move of the ions in the Monte Carlo simulation procedure. In our simulations we have adopted a more efficient computational strategy and data management scheme. Prior to starting the simulation we compute and tabulate the effective ion-ion interaction potential energies for a series of electron densities ranging from somewhat below to somewhat above the bulk density of liquid metal. During the simulation the interaction between a particular pair of ions is obtained from a rational functional interpolation for the given electron density using the precalculated data bank.

The model system for the simulations consisted of a slab of 1000 ions. The dimensions of the simulation slab were $L_0\times L_0\times 2L_0$ in the (x,y,z) directions. The slab contains two free surfaces in the positive z and negative z directions (normal to the two liquid-vapor interfaces), so that the area of each of the two liquid-vapor interfaces is $\sigma=L_0^2$. Periodic boundary conditions are applied in the x and y directions. In fact, periodic boundary conditions were also applied in the z direction, but at distances so far from the liquid-vapor interfaces that the description of those interfaces as free is valid. The size of the slab L_0 was chosen such that the average density of ions in the slab matched the density of the binary alloy at the simulation temperature. The center of mass of the simulation system was located at the origin of the coordinates $(x=0,y=0,z=0)$. The initial ion configuration was generated by placing the particles within the boundaries of the slab, subject to the constraint that no ion-ion separation was less than the ionic diameter.

The simulations were carried out using the Metropolis scheme[31] and a force bias Monte Carlo algorithm[4,9] to eliminate the overlaps between ion cores. The trial configurations were generated by randomly displacing a selected ion; the magnitude of the ionic displacement was chosen to lead to convergence to equilibrium with a reasonable overall acceptance ratio for the trial configurations.

IV. RESULTS OF CALCULATIONS

A. Alloy composition

We have carried out self-consistent Monte Carlo simulations of the structure of the liquid-vapor interface of liquid SnGa alloys at 57 °C; the available experimental data refer to this temperature. The simulations were carried out on an SGI-Origin 200 parallel computer. We define a simulation

pass to be 1000 ionic configurations. Using this unit, the simulations were carried out for up to 79 000 passes. The results we report here were obtained as an average over all the passes except the initial 5000.

Before describing the results of our simulations it is instructive to make a few remarks concerning the composition of the simulation samples. The experimental data were obtained from studies of an alloy with composition $Sn_{0.09}Ga_{0.91}$. To mimic this macroscopic composition, a double ended simulation sample such as we have used, and containing only 1000 atoms, would have far too few Sn atoms to generate the full monolayer coverage observed to occur in the liquid-vapor interface. This anomaly is a consequence of the limited size of the simulation sample. Unfortunately, it is not possible to carry out simulations with samples much larger than what we have used. We have addressed this difficulty in the same fashion as in our earlier studies of segregation in the liquid-vapor interface of GaBi alloys. Since the Sn atoms that segregate in the liquid-vapor interface are drawn from everywhere in the bulk alloy, we can mimic the real system with a small simulation sample by providing a total number of solute atoms that suffices to both cover the interface and be at the correct bulk concentration. Of course, the concentration of Sn atoms needed to create this mimic system exceeds the experimental concentration. Provided that the pseudopotential representation is accurate, the net result is that the segregated Sn will be atop a short column of bulk alloy with the equilibrium composition.

Adopting this point of view, we have used 1000 atom simulation samples with numbers of Sn atoms sufficient to generate the necessary surface density of segregated Sn in the liquid-vapor interface. Specifically, we have carried out simulations of the structures of the bulk liquid alloy and of the liquid-vapor interfaces of the mixtures with compositions $Sn_{0.09}Ga_{0.91}$and $Sn_{0.18}Ga_{0.82}$.

B. The transverse pair correlation function

The structure of the liquid-vapor interface is conveniently characterized by the transverse (in-plane) pair correlation function and the longitudinal density distribution. The transverse pair correlation function, which was calculated from a histogram of the separations of all pairs of particles in a thin slice of the interfacial region in the normalized correlation function form, is given by

$$g(r)=\frac{2V_T N(r,\Delta r)}{V_s N_T^2}, \tag{40}$$

where N_T is the total number of particles in the slice, $N(r,\Delta r)$ is the average number of pairs of particles between r and $r+\Delta r$ and in the slice, V_T is the total volume of all the

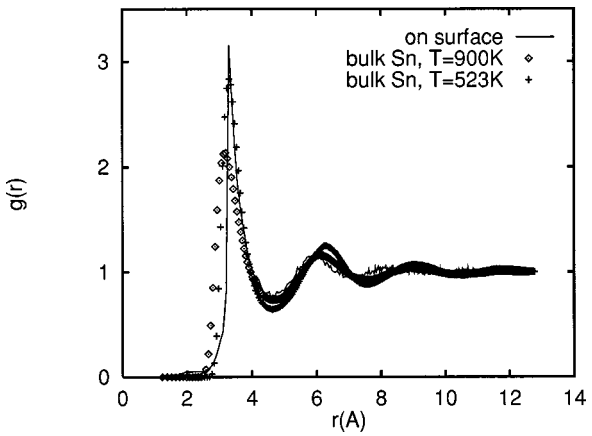

FIG. 5. Comparison of the pair correlation function in the liquid-vapor interface with that of bulk liquid Sn.

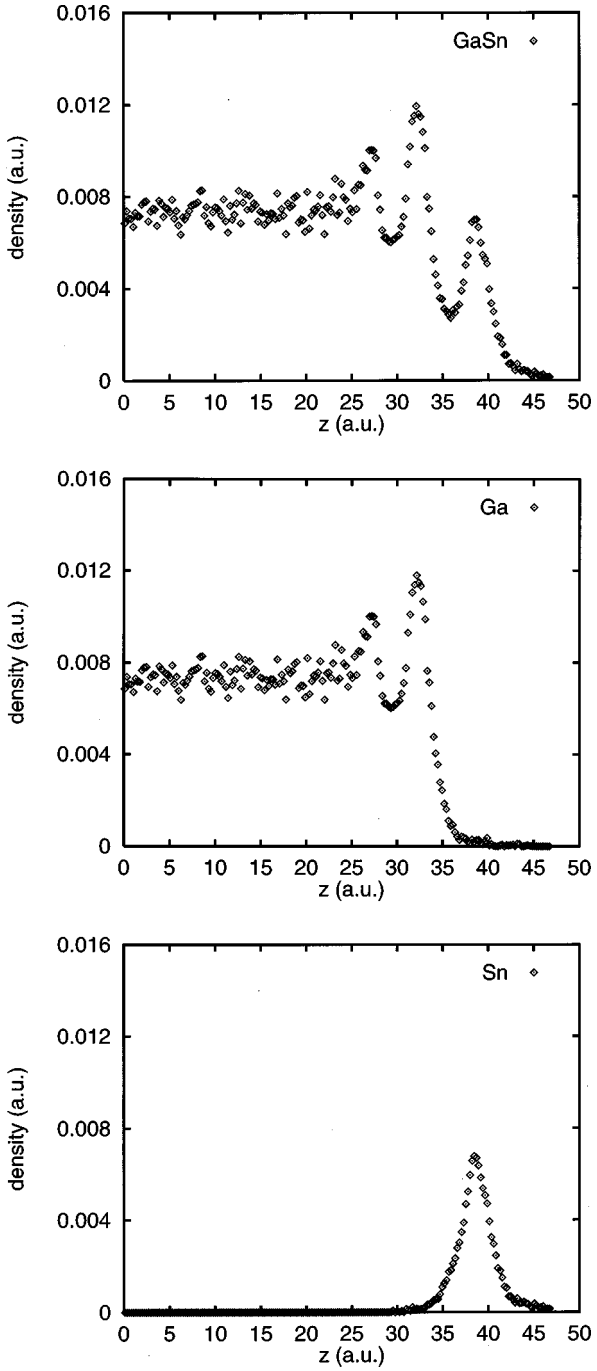

FIG. 6. Longitudinal density profiles in the liquid-vapor interface of $Sn_{0.09}Ga_{0.91}$; (a) the total atom density; (b) Ga; (c) Sn.

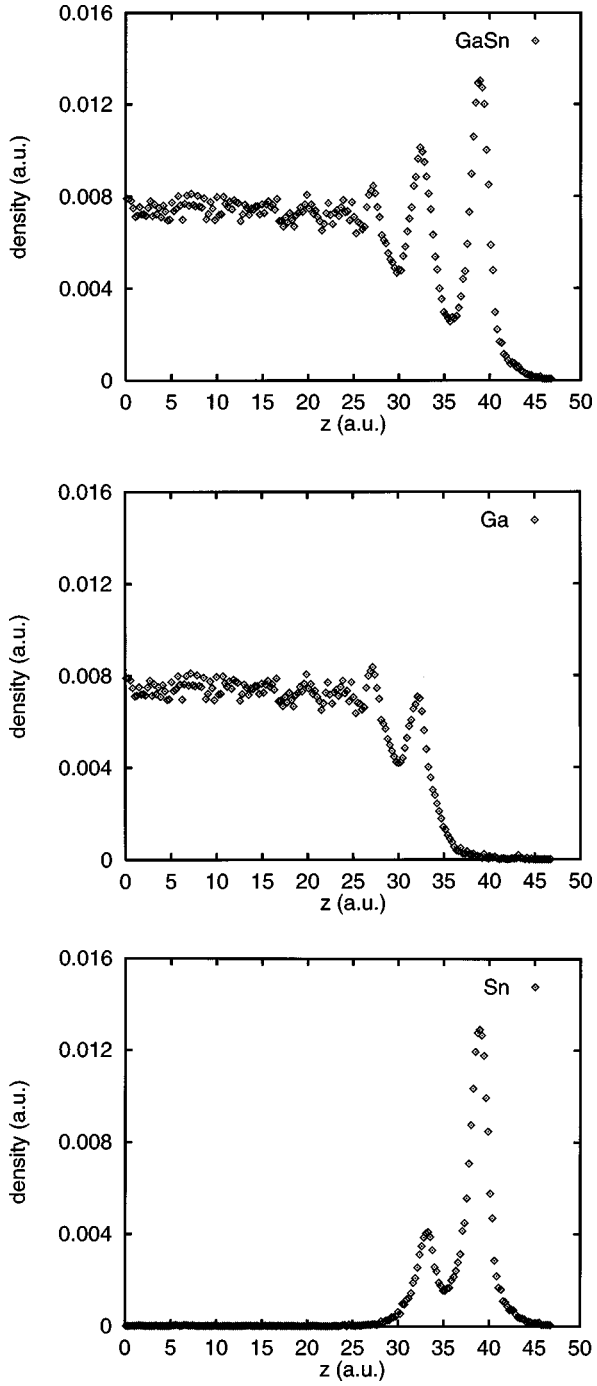

FIG. 7. Longitudinal density profiles in the liquid-vapor interface of $Sn_{0.18}Ga_{0.82}$; (a) the total atom density; (b) Ga; (c) Sn.

particles in the slice, and V_s is the average volume of the intersection of the spherical shell between r and $(r+\Delta r)$ of the thin slice.

We show in Fig. 4 the pair correlation functions in the bulk liquid for $Sn_{0.09}Ga_{0.91}$alloy. Figure 5 compares the calculated transverse pair correlation function of the segregated Sn in the liquid-vapor interface of the alloy with that of the supercooled bulk liquid. At $T=900$ K, the first peak of the bulk liquid pair correlation function is significantly smaller than that at $T=523$ K, and that of the calculated pair correlation function in the liquid-vapor interface. For the pair correlation function of liquid Sn at $T=523$ K, there is not any

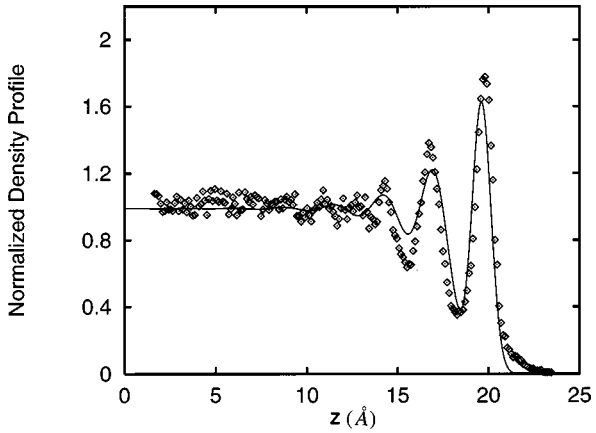

FIG. 8. Comparison of the predicted (□□□) and experimental (—) longitudinal density profiles in the liquid-vapor interface of a SnGa alloy (see text).

significant difference between the bulk liquid pair correlation function and the calculated pair correlation function in the liquid-vapor interface.

C. The longitudinal density distribution

The prediction of the longitudinal density distribution provides the most sensitive test of our calculations, and provides the most meaningful results for the confirmation of the experimental observation. The longitudinal density distribution of the ions was obtained from a histogram of the distance between a particle and the center of the mass of the slab; the density profiles in the $+z$ and the $-z$ directions were averaged to obtain the reported density distribution. We show in Fig. 6 the calculated longitudinal density profiles for $Sn_{0.09}Ga_{0.91}$ alloy, and in Fig. 7 the calculated longitudinal density profiles for $Sn_{0.18}Ga_{0.82}$ alloy.

D. Comparison to the experiment

The experimental studies[11] of the liquid-vapor interface of $Sn_{0.09}Ga_{0.91}$ at various temperatures referred to previously show that the Sn which segregates in the interface is distributed as a sensibly complete monolayer atop the bulk alloy and about 22% of the second layer. As already noted, to make a comparison between the simulation results and the experimental data we must use a simulation sample for which the Sn fills the outermost layer of the liquid-vapor interface and then about 22% of the second layer. For this purpose we use the simulation sample with composition $Sn_{0.18}Ga_{0.82}$. We show a comparison of the calculated and experimental longitudinal density distributions in Fig. 8.

The agreement between the predicted and observed longitudinal density distributions in the liquid-vapor interface of $Sn_{0.09}Ga_{0.91}$ is very good, but the predicted amplitude modulation of the longitudinal density distribution is somewhat greater than that observed. The results of our simulations suggest that the presence of the Sn monolayer alters the longitudinal density distribution of the underlying liquid Ga to some extent. As in our previous study of the longitudinal

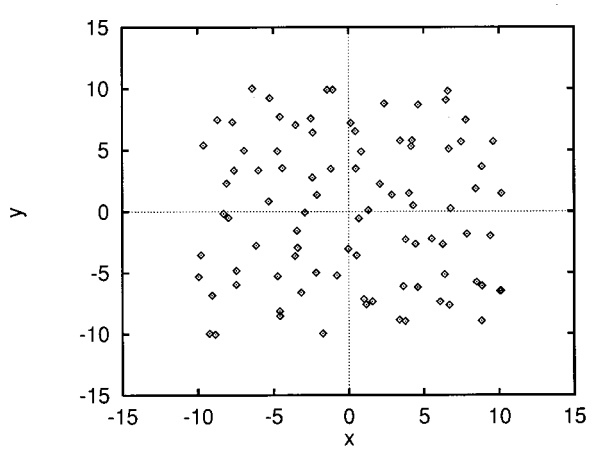

FIG. 9. The relative positions of the Sn atoms in the x-y plane of the outermost layer of the liquid-vapor interface of $Sn_{0.09}Ga_{0.91}$.

density distribution[9] in the liquid-vapor interface of GaBi, we attribute the overshoot of the theoretical peak amplitudes to the inability of the simulation sample to support the long wavelength capillary waves which are believed to determine the temperature dependences of the amplitudes and widths of the peaks in the longitudinal density distribution.

We show in Fig. 9 the coordinates in the x-y plane of the centers of the Sn atoms on the outmost layer of the liquid-vapor interface of the alloy with composition $Sn_{0.09}Ga_{0.91}$. This figure provides supplementary verification that the structure of the segregated layer of Sn is that of a liquid.

V. FINAL REMARK

We have shown that self-consistent Monte Carlo simulations of the structure of the liquid-vapor interface of a SnGa alloy reproduce all of the unusual features observed experimentally. In particular, the use of an effective valence approximation in the simulation of heterovalent alloys is shown to be sufficiently accurate to be useful for the calculation of the structure of an alloy which does not exhibit compound formation.

ACKNOWLEDGMENT

This work has been supported by a grant from the National Science Foundation.

[1] M. P. D'Evelyn and S. A. Rice, Phys. Rev. Lett. **47**, 1844 (1981).
[2] M. P. D'Evelyn and S. A. Rice, J. Chem. Phys. **78**, 5081 (1983).
[3] M. P. D'Evelyn and S. A. Rice, J. Chem. Phys. **78**, 5225 (1983).
[4] J. G. Harris, J. Gryko, and S. A. Rice, J. Chem. Phys. **87**, 3069 (1987).
[5] J. G. Harris, J. Gryko, and S. A. Rice, J. Stat. Phys. **48**, 1109 (1987).
[6] N. Lei, Z. Huang, and S. A. Rice, J. Chem. Phys. **104**, 4802 (1996).
[7] N. Lei, Z. Huang, S. A. Rice, and C. Grayce, J. Chem. Phys. **105**, 9615 (1996).
[8] M. J. Regan, P. S. Pershan, O. M. Magnussen, B. M. Ocko, M. Deutsch, and L. E. Berman, Phys. Rev. B **55**, 15874 (1997).
[9] M. Zhao, D. Chekmarev, and S. A. Rice, J. Chem. Phys. **108**, 5055 (1998).
[10] S. A. Rice and M. Zhao, Phys. Rev. B **57**, 13501 (1998).
[11] N. Lei, Z. Huang, and S. A. Rice, J. Chem. Phys. **107**, 4051 (1997).
[12] A. Gomez and S. A. Rice, J. Chem. Phys. **101**, 8094 (1994).
[13] M. Zhao, D. Chekmarev, Z. Cai, and S. A. Rice, Phys. Rev. E **56**, 7033 (1997).
[14] S. A. Rice, M. Zhao, and D. Chekmarev, *Proceedings of MRS*, December 1997.
[15] M. Zhao, D. Chekmarev, and S. A. Rice, J. Chem. Phys. **109**, 768 (1998).
[16] M. Zhao and S. A. Rice, Int. J. Chem. **1**, URL: http://www.ijc.com/articles/1998v1/1 (1998).
[17] D. Chekmarev, M. Zhao, and S. A. Rice, J. Chem. Phys. **109**, 1959 (1998).
[18] D. Chekmarev, M. Zhao, and S. A. Rice, Phys. Rev. E **59**, 479 (1999).
[19] T. L. Gilbert, J. Chem. Phys. **49**, 2640 (1968).
[20] R. W. Shaw, Jr., Phys. Rev. **174**, 764 (1968).
[21] N. H. March, Adv. Phys. **6**, 1 (1957).
[22] D. A. Kirzhnits, Sov. Phys. JETP **5**, 64 (1957).
[23] S. H. Vosko, L. Wilk, and M. Nusair, Can. J. Phys. **58**, 1200 (1980).
[24] D. C. Langreth and M. J. Mehl, Phys. Rev. B **28**, 1809 (1983).
[25] C. H. Woo, S. Wang, and M. Matsuura, J. Phys. F **5**, 1836 (1975).
[26] W. Kohn and L. J. Sham, Phys. Rev. A **140**, 1133 (1965).
[27] P. Hohenberg and W. Kohn, Phys. Rev. B **136**, 864 (1964).
[28] A. K. Karmakar and R. N. Joarder, Phys. Bl. **245**, 81 (1998).
[29] A. G. Eguiliz, D. A. Campbell, A. A. Maradudin, and R. F. Wallis, Phys. Rev. B **30**, 5449 (1984).
[30] J. P. Perdew, M. Ernerhof, A. Zupan, and K. Burke, J. Chem. Phys. **108**, 1522 (1998).
[31] N. Metropolis, A. W. Rosenbluth, M. N. Rosenbluth, A. M. Teller, and E. Teller, J. Chem. Phys. **21**, 1087 (1953).